

The BiomolBiomed publishes an “Advanced Online” manuscript format as a free service to authors in order to expedite the dissemination of scientific findings to the research community as soon as possible after acceptance following peer review and corresponding modification (where appropriate). An “Advanced Online” manuscript is published online prior to copyediting, formatting for publication and author proofreading, but is nonetheless fully citable through its Digital Object Identifier (doi®). Nevertheless, this “Advanced Online” version is NOT the final version of the manuscript. When the final version of this paper is published within a definitive issue of the journal with copyediting, full pagination, etc., the new final version will be accessible through the same doi and this “Advanced Online” version of the paper will disappear.

RESEARCH ARTICLE

Ding et al: Methylene blue reduces lung injury in HCA rats

Methylene blue mitigates lung injury in HCA rats by regulating macrophage pyroptosis via Nrf2/HO-1 and NLRP3 pathways

Fuyan Ding¹, Hong Wang¹, Gang Qiao², Zhidong Zhang^{2*}

¹Department of Vascular Diseases Intensive Care Unit, Zhengzhou University Central China Fuwai Hospital, People’s Hospital of Zhengzhou University, Henan, China

²Department of Vascular Surgery, Zhengzhou University Central China Fuwai Hospital, People’s Hospital of Zhengzhou University, Henan, China

*Correspondence to **Zhidong Zhang**, e-mail: 15838127197@163.com

DOI: <https://doi.org/10.17305/bb.2025.11851>

ABSTRACT

Methylene blue (MB) has antioxidant properties, yet its role in acute lung injury (ALI) induced by hypothermic circulatory arrest (HCA) remains unexplored. This study investigates MB's effects and underlying regulatory mechanisms in an HCA rat model. Rats received an intravenous bolus of MB (1 mg/kg) 15 minutes before HCA induction. Physiological parameters were monitored, and bronchoalveolar lavage fluid (BALF) was collected 2 hours postoperatively to assess total protein levels, inflammatory cells, and cytokines. Histopathological lung damage was evaluated using hematoxylin-eosin (H&E) and TUNEL staining. Inflammatory markers and oxidative stress indicators were measured via ELISA and DHE staining. Alveolar macrophages (AMs) were isolated to analyze polarization using flow cytometry and immunofluorescence double staining. Pyroptosis in AMs was detected with Yo-Pro-1 and Hoechst 33342 staining. Additionally, Western blotting was performed to examine the Nrf2/HO-1 pathway, Nod-like receptor protein 3 (NLRP3) inflammasome, and pyroptosis-related proteins. Following HCA, rats exhibited significant blood gas abnormalities, structural lung damage, increased pathological scores, and higher apoptosis rates. However, MB mitigated these effects, improving physiological parameters and reducing lung histopathology scores. MB also lowered pro-inflammatory cytokine levels, increased SOD and GSH-Px activity, promoted AM polarization toward the M2 phenotype, and decreased pyroptosis. Mechanistically, MB activated the Nrf2/HO-1 pathway while inhibiting NLRP3 inflammasome activation. Notably, Nrf2 inhibitors and NLRP3 agonists weakened MB's protective effects by promoting inflammasome activation and pyroptosis, whereas Nrf2 agonists and NLRP3 inhibitors enhanced MB's beneficial impact. In conclusion, MB attenuates HCA-induced ALI by modulating AM polarization and pyroptosis via Nrf2/HO-1 pathway activation and NLRP3 inflammasome inhibition.

Keywords: Methylene blue; MB; hypothermic circulatory arrest; HCA; NLRP3 inflammasome; Nrf2/HO-1 pathway; pyroptosis.

INTRODUCTION

Hypothermic circulatory arrest (HCA) is a complex cardiopulmonary bypass (CPB) technique that has become essential for open-heart surgery since its introduction in the 1950s [1,2]. By lowering tissue metabolism and oxygen consumption, HCA enhances the body's tolerance to ischemia and hypoxia while also providing a relatively bloodless surgical field, which increases the chances of success [3,4]. Despite continuous advancements in CPB tubing materials and HCA techniques, many patients still experience postoperative complications of varying severity, including acute lung injury (ALI), neurocognitive dysfunction, and acute kidney injury [5-7]. Notably, the incidence of ALI exceeds 35% [8]. The mechanisms underlying HCA-induced ALI are complex and involve oxidative stress from reactive oxygen species (ROS), systemic inflammatory responses, and lung ischemia/reperfusion injury [9,10]. Alveolar macrophages (AMs), the primary immune cells in lung tissue, play a crucial role in inflammation, and their death exacerbates ALI progression [11,12]. Pyroptosis, a form of programmed inflammatory cell death primarily mediated by gasdermin-D (GSDMD), has been implicated in ALI, cardiovascular diseases, and cancer [13-15]. The interaction between AM pyroptosis and inflammation further amplifies lung tissue damage, disrupting alveolar structure and homeostasis, ultimately contributing to ALI onset and progression [16]. The Nod-like receptor protein 3 (NLRP3) inflammasome, which consists of NLRP3, caspase-1, and apoptosis-associated speck-like protein (ASC), is a key component of the innate immune system and plays a central role in metabolic inflammatory responses [17,18]. Activated caspase-1 generates the N-terminal fragment of GSDMD (GSDMD-N), which ultimately triggers pyroptosis [19]. Therefore, inhibiting AM pyroptosis mediated by the NLRP3 inflammasome is crucial for mitigating HCA-induced ALI.

Methylene blue (MB) is an aromatic compound with a heterocyclic structure that

serves various functions in both biology and chemistry, including its use as a dye in the textile industry [20]. Notably, MB has a low redox potential (11 mV), which enables it to catalyze redox reactions and reduce ROS production [20]. Clinically, MB has demonstrated efficacy in treating conditions such as carbon monoxide poisoning, methemoglobinemia, infectious shock, and urinary tract infections, among others [21–23]. Additionally, MB exhibits anti-inflammatory properties by reducing nitric oxide synthase activity and inhibiting inflammatory signaling, thereby providing neuroprotection [24]. In support of this, microglia exposed to lipopolysaccharide showed a reduction in inflammatory gene expression when MB was introduced to the culture medium [25]. However, no studies have explored the role of MB in NLRP3 inflammasome activation, pyroptosis of AMs, or the associated regulatory mechanisms. Nuclear factor erythroid-2 related factor 2 (Nrf2) is a key modulator of cellular antioxidant responses, regulating the expression of antioxidant, anti-inflammatory, and detoxification-related genes [26]. Under oxidative stress, cytoplasmic Nrf2 dissociates from Keap1 and translocates into the nucleus, where it enhances the expression of heme oxygenase-1 (HO-1) [27]. Activation of the Nrf2/HO-1 pathway has been shown to mitigate inflammation and oxidative stress-related damage in various diseases [28–30]. However, whether MB can alleviate lung injury caused by HCA by activating the Nrf2/HO-1 pathway remains unknown. In this study, we established an HCA-induced acute lung injury (ALI) rat model to investigate whether MB attenuates ALI by inhibiting the pyroptosis of AMs and its associated regulatory mechanisms. Our findings aim to provide theoretical support for the potential use of MB in ALI management.

MATERIALS AND METHODS

Animal feeding

Healthy male SD rats (5 per cage) were obtained from Vital River Laboratory Animal Technology Co., Ltd. (Beijing, China) and housed in a standard animal breeding room

for a one-week acclimation period. The room temperature was maintained at 22 ± 2 °C with a relative humidity of 45%. The rats had free access to food and water. All facilities, including food containers, cages, water bottles, and drinking spouts, were regularly sterilized. All animal experiments were approved by the Zhengzhou University Animal Ethics and Welfare Committee (Approval No. 2022 Ethics (33)) and conducted in accordance with the Code of Ethics for Laboratory Animals.

Animal grouping and treatment

SD rats were randomly divided into seven groups (n=30/group): sham, HCA, HCA+MB, HCA+MB+TBHQ (TB), HCA+MB+ML385 (ML), HCA+MB+Nigericin (Nig), and HCA+MB+MCC950 (MCC). Sham group: Rats underwent anesthesia, tracheal intubation, ventilation, and vascular cannula placement. HCA group: Rats received CPB and HCA treatment. HCA+MB group: Rats received methylene blue (MB, 1 mg/kg, M9140, Sigma-Aldrich, St. Louis, MO, USA) via push administration 15 minutes before HCA induction [31]. HCA+MB+TB group: The Nrf2 agonist TB (20 mg/kg, HY-100489, MedChemExpress, Monmouth Junction, NJ, USA) was administered intraperitoneally 1 hour before HCA induction, and MB was given 15 minutes before HCA induction [31]. HCA+MB+ML group: The Nrf2 inhibitor ML (30 mg/kg, HY-100523, MedChemExpress) was administered intraperitoneally 1 hour before HCA induction, followed by MB 15 minutes prior [32]. HCA+MB+Nig group: The NLRP3 agonist Nigericin (Nig, 1 mg/kg, HY-127019, MedChemExpress) was administered intraperitoneally 1 hour before HCA induction, with MB given 15 minutes prior [32]. HCA+MB+MCC group: The NLRP3 inhibitor MCC950 (MCC, 10 mg/kg, HY-12815, MedChemExpress) was administered intraperitoneally 1 hour before HCA induction, with MB given 15 minutes prior [33].

Construction of HCA rat model

Referring to the methods of Linardi et al. [34] and Li et al. [35], rats were anesthetized via intraperitoneal injection of sodium pentobarbital (50 mg/kg, P3761,

Sigma-Aldrich) and intubated with a 16-gauge cannula before being connected to an animal ventilator. To maintain anesthesia, 1.5% sevoflurane was administered, and mechanical ventilation was set to a tidal volume of 8 mL/kg with a respiratory rate of 60 breaths/min. These parameters were dynamically adjusted based on blood gas analysis results (GEM3500, Radiometer, Copenhagen, Denmark). A pre-heparinized 24-gauge catheter was inserted into the left superficial femoral artery to administer sodium heparin (500 IU/kg) for systemic anticoagulation. Simultaneously, the catheter was connected to a multifunctional physiological monitor (PowerLab, Harvard Apparatus, USA) to measure heart rate and mean arterial pressure (MAP). A venous drain with 24 lateral holes (created using a 12-gauge needle) was inserted into the right external jugular vein to serve as an outlet for venous blood flow. Meanwhile, a 20-gauge catheter was placed in the middle caudal artery to facilitate arterial blood inflow into the CPB circuit. Rectal temperature was continuously monitored using a temperature probe (PowerLab, Harvard Apparatus, USA). Following the method of Kong et al. [9], rats underwent CPB and HCA. Blood drained from the jugular vein entered a venous reservoir before being transported via a rolling blood pump to a membrane oxygenator for gas exchange. After heat exchange, the blood was returned to the body through the caudal artery. Once CPB was established, cooling was initiated using a heat exchanger combined with ice packs for 30 minutes. When the rectal temperature reached 25°C, CPB and ventilation were completely halted, inducing 30 minutes of circulatory arrest, during which all organs experienced ischemic and hypoxic conditions under hypothermia. At the end of the circulatory arrest period, CPB and mechanical ventilation were restarted. A heating blanket was used to gradually raise the rectal temperature to 35°C over 30 minutes. Once this temperature was reached, CPB and anesthesia were discontinued, and oxygen-enriched mechanical ventilation was maintained for an additional 60 minutes to allow full recovery from anesthesia. During the resuscitation phase, the remaining perfusion solution was gradually administered to maintain MAP above 80

mmHg. Thirty minutes postoperatively, MAP was measured, and 1 mL of blood was collected from the abdominal aorta for arterial blood gas analysis.

Determination of total protein concentration

Two hours after CPB surgery, six rats from each group were randomly selected and euthanized via sodium pentobarbital injection (100 mg/kg). Lung tissues were isolated, and bronchoalveolar lavage fluid (BALF) was collected. The right lower lobe of each rat's lung was removed and placed in a single-use petri dish on ice. The bronchus was identified, secured, and cannulated with a 20 G indwelling needle attached to a 1 mL syringe, then ligated. BALF was obtained by three consecutive lavages with 1 mL of 4°C PBS. The collected fluid (about 0.7 mL) was centrifuged, and the supernatant was stored at -80°C for further analysis. Total protein concentration in BALF supernatants was measured using a bicinchoninic acid (BCA) Protein Assay Kit (P0012, Beyotime, Shanghai, China).

Neutrophil and macrophage count

Following the method of Kalidhindi et al. [36], the collected BALF (1 mL) was centrifuged, and the precipitate was resuspended in 1 mL of PBS. The sample was washed again by centrifugation to remove excess washings. A 3 µL smear of the cell sediment was prepared, and Diff-Quik staining solution (G1540, Solarbio, Beijing, China) was added dropwise to cover the smear for 1 minute. Macrophages and neutrophils were counted under a light microscope using a haematocrit counter (Z359629, Sigma-Aldrich), with a total of 200 cells analyzed.

Measurement of lung dry/wet weight ratio

Immediately after the removal of the left upper lung lobe from the rats, the tissue was blotted with filter paper to remove surface fluid. Its wet weight (W) was then measured and recorded. The tissue was subsequently dried at 58°C for 48 hours, after which the dry weight (D) was recorded. Finally, the W/D ratio was calculated.

Hematoxylin and eosin (HE) staining

To detect lung tissue lesions in rats, an HE staining kit (C0105S, Beyotime) was used. Lung tissue samples were fixed in 10% neutral formalin solution (F5554, Sigma-Aldrich) for 24 hours and then dehydrated in a graded ethanol series (100%, 95%, 75%, and 50%). The samples were embedded in paraffin, sectioned at 4 μm , and baked at 65°C for 8 hours. The sections were then deparaffinized with xylene (247642, Sigma-Aldrich) and washed with distilled water. Staining was performed using hematoxylin staining solution for 8 minutes, differentiation solution (C0161S, Beyotime) for 30 seconds, and eosin staining for 1 minute. The sections were sequentially dehydrated in ethanol at different concentrations, cleared with xylene, sealed, and finally examined under an inverted microscope (DM IL LED, Leica, Heidelberg, Germany).

Histological assessment of lung injury

In each group of rats, histological examination of lung injury was conducted following the methods of Hirao et al. [37] and Li et al. [38]. The severity of lung injury was assessed by quantifying four key indicators: (I) inflammatory cell infiltration, (II) interstitial edema, (III) alveolar septal congestion, and (IV) alveolar hemorrhage. Each parameter was scored on a scale from 0 to 4, with higher scores indicating more severe injury. The total histopathological score was obtained by summing the four individual scores.

TUNEL staining

Wax blocks of rat lung tissue were routinely sectioned, deparaffinized with xylene, and dehydrated using a gradient ethanol series. DNase-free proteinase K (20 $\mu\text{g}/\text{mL}$, ST532, Beyotime) was added dropwise, and the samples were incubated for 30 min, followed by three washes with PBS. TUNEL assay solution (C1086, Beyotime) was then added dropwise and incubated for 1.5 h. Subsequently, the samples were stained

with DAPI solution (D9542, Sigma-Aldrich) for 10 min in darkness. After sealing with anti-fade mounting medium (HY-K1042, MedChemExpress), an inverted fluorescence microscope was used for observation and imaging.

Detection of cellular ultrastructure by transmission electron microscopy

Lung tissues were collected and fixed in 2.5% glutaraldehyde (G6257, Sigma-Aldrich) at 4°C overnight. After two rinses with PBS, the samples were treated with 1% osmium tetroxide (O5500, Sigma-Aldrich) for 2 hours. Dehydration was carried out using a graded ethanol series (30%, 50%, 70%, 80%, 95%, and 100%) for 10 minutes at each step, followed by two final dehydration steps with 100% acetone for 10 min each. The samples were then embedded and polymerized at 60°C for 48 hours. Thin sections (60 nm) were prepared and subjected to double staining with 2% uranyl acetate and lead citrate. After drying, they were mounted on copper grids and observed using a transmission electron microscope (Spectra 200 TEM, Thermo Fisher Scientific), with images recorded accordingly.

ELISA

Rat lung tissues were cut, thoroughly ground with saline, and centrifuged to collect the supernatant. The levels of superoxide dismutase (SOD, ml077379), malondialdehyde (MDA, ml077384), myeloperoxidase (MPO, ml003250), and glutathione peroxidase (GSH-Px, ml097316) in lung tissue supernatants, as well as intercellular adhesion molecule-1 (ICAM-1, ml003031), interleukin (IL)-6, tumor necrosis factor-alpha (TNF- α , ml002859), and IL-10 (ml002813) in BALF, were assessed using ELISA. All kits were obtained from Enzyme Link Biotechnology (Shanghai, China). Tissue or BALF supernatants were added to the ELISA well plate, followed by the corresponding antibody, and incubated for 1.5 h. After incubation, the antibody solution was discarded, and the wells were washed three times with washing buffer. The washing solution was removed, and the wells were exposed to streptavidin-HRP for 30 minutes. Substrates A and B were then added and incubated

for 10 minutes. Finally, the termination solution was added, mixed, and the OD450 value was measured immediately using a microplate reader (1410101, Thermo Fisher Scientific, Waltham, MA, USA).

Determination of ROS levels in lung tissue

Frozen rat lung tissue sections, prepared within 1 h of excision, were treated with a drop of cleaning solution spread evenly across the entire surface and left to stand for 5 min. After aspirating the solution, a 10 μ M Dihydroethidium (DHE) probe (S0063, Beyotime) was applied dropwise to ensure uniform coverage and incubated in darkness for 30 minutes. The sections were then washed twice with PBS, covered with cover slips, and observed under an inverted microscope. Images were captured and analyzed using ImageJ software (version 1.45, Wayne Rasband, National Institute of Mental Health, USA).

Flow cytometry

The percentage of AM polarization was determined using the method described by Hwang et al. [39]. The obtained BALF was filtered through cell filters, centrifuged, and counted. The resulting cell suspension was added to Percoll Density Gradient Separation Solution (P4937, Sigma-Aldrich) and subjected to gradient centrifugation according to the reagent instructions. The cell layer at the gradient interface was collected, and the isolated cells were washed with PBS to remove any remaining density gradient separator. The washed cell suspension was then seeded into 6-well plates, and an appropriate amount of DMEM medium (11965092, Gibco, Grand Island, NY, USA) containing 10% fetal bovine serum (F0193, Sigma-Aldrich) was added. Cells were cultured at 37°C with 5% CO₂ for 2–3 hours to allow macrophages to adhere. The medium was gently aspirated, and the cells were washed twice with PBS to remove non-adherent cells. Next, 200 μ L of a cell suspension containing 1×10^5 macrophages was taken, and 5 μ L of FITC-labeled CD68 primary antibody (11-0689-42, Invitrogen, Carlsbad, CA, USA) and CD163 primary antibody

(11-1631-82, Invitrogen) were added separately. The mixture was incubated at 4°C for 30 minutes in the dark. After incubation, 5 mL of sample buffer was added, mixed thoroughly, and centrifuged for 5 minutes. The precipitate was collected, resuspended in 200 µL of sample buffer, and analyzed using flow cytometry (BD FACSCalibur™, BD Biosciences, San Jose, CA, USA) to detect fluorescence signals and evaluate the expression of relevant markers for macrophage proportion analysis.

Immunofluorescence

Following the method of Dai et al. [40], paraffin sections of rat lung tissue were deparaffinized with xylene and dehydrated using a gradient ethanol series. The sections were then placed in 0.1 mol/L citrate buffer (pH = 6, S1804, Sigma-Aldrich) for antigen retrieval, microwaved on medium heat for 6 minutes until reaching a slight boil, and then maintained at medium-low heat for an additional 10 minutes. The heating was then stopped, and the sections were allowed to cool naturally for 20 minutes. To permeabilize the tissue sections, 0.3% Triton X-100 (X100, Sigma-Aldrich) was applied for 10 minutes. Afterward, the sections were blocked with 5% bovine serum albumin (BSA, V900933, Sigma-Aldrich) for 30 minutes. They were then incubated overnight at 4°C with one of the following primary antibodies to evaluate changes in M1 and M2 macrophage proportions: inducible nitric oxide synthase (iNOS) (PA1-036, 1:50, Invitrogen), CD163 (MA5-16656, 1:100, Invitrogen), or CD68 (14-0688-82, 1:50, Invitrogen). To assess the Nrf2/HO-1 pathway, the sections were incubated overnight at 4°C with either Nrf2 primary antibody (PA5-27882, 1:100, Invitrogen) or HO-1 primary antibody (PA5-77833, 1:100, Invitrogen). On the following day, FITC-labeled secondary antibody (sheep anti-rabbit IgG, F-2765, 1:100, Invitrogen) was added and incubated for 1 hour in darkness. Finally, DAPI staining solution was applied for 10 min, after which the sections were blocked and observed under a fluorescence microscope.

Yo-Pro-1 staining and Hoechst 33342 staining

Following the method of Han et al. [41], AMs were collected from each group, and an appropriate amount of Yo-Pro-1 staining solution (200 nM, C1356S, Beyotime) was added to each well, ensuring the dye covered the cell surface. The cells were incubated for 15 minutes at room temperature, protected from light. Subsequently, nuclei were stained with Hoechst 33342 staining solution (10 µg/mL, C1022, Beyotime) and incubated for 30 minutes to indicate the total cell number. Under fluorescence microscopy, Yo-Pro-1 produced green fluorescence upon entering pyroptotic cells, while Hoechst 33342 staining resulted in blue fluorescence in the nuclei.

Western blot

Rat lung tissues and AMs were thoroughly ground, followed by lysis with RIPA buffer (P0013B, Beyotime) to extract proteins. Protein concentrations were quantified using a BCA assay kit. The samples were then subjected to electrophoresis on 12% SDS-PAGE gels (Invitrogen), transferred onto polyvinylidene difluoride (PVDF) membranes (Invitrogen), and blocked with 5% BSA for 3 h. After washing, the membranes were incubated overnight at 4°C with the following primary antibodies: Nrf2 (PA5-27882, 1:500, Invitrogen), HO-1 (PA5-77833, 1:1000, Invitrogen), NLRP3 (MA5-23919, 1:100, Invitrogen), pro-caspase-1 (ZRB1233, 1:1000, Sigma-Aldrich), caspase-1 (MA5-16215, 1:200, Invitrogen), ASC (HY-P80548, 1:500, MedChemExpress), GSDMD-N (ab215203, 1:1000, Abcam), or GSDMD (PA5-116815, 1:1000, Invitrogen). The next day, membranes were incubated with a secondary antibody (ab205718, 1:10,000, Abcam) for 2 hours. A chemiluminescent substrate (ECL, 34580, Thermo Fisher Scientific) was evenly applied to the membranes, and protein bands were visualized using a gel imaging system (iBright CL1500, Invitrogen). GAPDH (ab263962, 1:1000, Abcam) served as an internal control. Grayscale values of protein bands were quantified using ImageJ software.

Ethical statement

All rat experiments were approved by Zhengzhou University Animal Ethics and Welfare Committee (approval number: 2022 Ethics No. (33)) and followed the Code of Ethics for Laboratory Animals.

Statistical analysis

A minimum of three repetitions was performed for each experiment, with results presented as mean \pm standard deviation. Statistical analysis was conducted using SPSS 26.0 (IBM SPSS Statistics 26). Multiple group comparisons were performed using one-way analysis of variance (ANOVA). For independent samples, a Student's t-test was used if the data were normally distributed; otherwise, non-parametric tests were applied. A *P*-value of < 0.05 was considered statistically significant. Data visualization was carried out using GraphPad Prism 9.0.

RESULTS

MB ameliorates HCA-induced abnormalities in physiological indices in rats

At 30 minutes post-surgery, the MAP of rats was monitored using a multifunctional physiological monitor. Compared to Sham rats, HCA rats exhibited a significant decline in MAP, which was alleviated by MB injection (Figure 1A). Blood gas analysis revealed that both hemoglobin (Hb) and hematocrit (Hct) levels were markedly reduced in HCA rats, likely due to blood dilution from the perfusion of pre-filled fluid during the CPB procedure (Figures 1B–1C). Additionally, after HCA intervention, arterial partial pressure of oxygen (PaO₂) was notably reduced, while partial pressure of arterial carbon dioxide (PaCO₂) was significantly elevated. However, MB treatment effectively improved these abnormalities (Figures 1D–1E). Furthermore, lactic acid accumulation was observed in rats during the 30-minute HCA procedure, prompting the use of sodium bicarbonate to correct the resulting acidosis. Notably, MB treatment reduced lactate accumulation (Figures 1F–1G). These findings confirm the successful implementation of HCA as an interventional process

while demonstrating that MB mitigates the physiological abnormalities induced by HCA.

MB ameliorates HCA-induced histopathological lung injury in rats

To assess histological changes in the lungs of rats following HCA, we collected lung tissue samples and prepared BALF 2 hours after surgery. HCA intervention led to a significant increase in total protein content and the W/D ratio in rat BALF, whereas MB treatment reduced protein levels and alleviated lung edema (Figures 2A–2B). HE staining revealed alveolar hemorrhage, alveolar wall thickening, interstitial capillary dilation and congestion, interstitial edema, and a significantly higher pathological damage score in the HCA group (Figure 2C). MB treatment mitigated interstitial capillary dilation and congestion and significantly reduced pathology scores. HCA-induced lung tissue damage was further confirmed by an increase in TUNEL-positive cells and apoptosis rate, both of which were significantly reduced with MB treatment (Figure 2D). Additionally, transmission electron microscopy showed ultrastructural alterations in the alveoli of the HCA group, characterized by small vacuoles in the cytoplasm, mitochondrial edema, and irregular nuclear morphology. In contrast, the HCA+MB group exhibited significantly attenuated ultrastructural changes, with minimal cellular damage, more intact nuclear morphology, homogeneous cytoplasm, and a moderate number of organelles (Figure 2E). These findings indicate that MB significantly improves HCA-induced histopathological changes in the lungs.

MB ameliorates HCA-induced inflammatory and oxidative stress injury in rat

Following the surgical procedure, the HCA group exhibited a markedly elevated count of macrophages and neutrophils in BALF, indicating increased alveolar wall permeability and a significant inflammatory response in rats. However, MB treatment significantly reduced macrophage and neutrophil counts (Figures 3A–3B). ELISA findings revealed that MPO levels, a key inflammatory marker, were notably

increased in HCA rats, whereas the HCA+MB group showed a significant reduction in MPO levels (Figure 3C).

Additionally, the levels of inflammatory factors TNF- α , IL-6, and ICAM-1 were significantly elevated in the BALF of HCA rats, while the anti-inflammatory cytokine IL-10 was markedly reduced. MB treatment effectively mitigated these inflammatory changes (Figures 3D–3G). DHE staining further demonstrated that ROS levels were markedly increased in HCA rats, while MB injection significantly reduced ROS levels (Figure 3H). Moreover, HCA led to a decline in the activity of antioxidant enzymes (SOD and GSH-Px) and an increase in MDA levels, a marker of oxidative stress, in rat lung tissues. MB treatment significantly suppressed HCA-induced oxidative stress (Figures 3I–3K). These findings suggest that MB effectively inhibits HCA-induced lung inflammation and attenuates oxidative stress injury.

MB promotes polarisation of rat AMs towards the M2 type

Next, we examined the expression of AM polarization markers after MB treatment to explore its effect on AM polarization. Based on pre-experiment results, we isolated AMs from BALF with a purity exceeding 99%. Flow cytometry results showed that M2-type AMs were nearly absent in the BALF of HCA rats, whereas MB treatment significantly increased their percentage (Figure 4A). Immunofluorescence analysis revealed that HCA rats had a markedly higher number of CD68⁺ cells and a greater proportion of M1-type (iNOS⁺CD68⁺) cells in their lung tissues compared to the Sham group. This suggests that a large population of activated AMs was present in HCA rats, with the vast majority being M1-type (Figures 4B-4E). In contrast, MB treatment significantly reduced the proportion of M1-type AMs in HCA rats and promoted their polarization toward the M2 type, which may be a key mechanism underlying MB's effects.

MB activates the Nrf2/HO-1 pathway in HCA rats

Given the crucial role of the Nrf2/HO-1 pathway in inflammation and oxidative stress,

we hypothesized that MB's protective effects on rat lung tissue might be linked to this pathway. Our results showed that HCA significantly reduced Nrf2 and HO-1 levels in rat lung tissues, suggesting that HCA inhibits the Nrf2/HO-1 pathway (Figure 5A–5C). However, lung tissues from the HCA+MB group exhibited higher Nrf2 and HO-1 levels, indicating that MB activates this pathway. Western blot assay results further confirmed this, demonstrating a notable reduction in Nrf2 and HO-1 protein levels in HCA rats, while MB treatment restored these levels (Figure 5D–5F). These findings suggest that MB activates the Nrf2/HO-1 pathway in HCA-exposed rats.

MB inhibits NLRP3 inflammasome-induced pyroptosis in rat AMs

Research indicates that NLRP3 inflammasome activation and cellular pyroptosis are closely linked to the inflammatory pathological process of ALI [42, 43]. Yo-Pro-1 and Hoechst 33342 staining revealed a significant increase in Yo-Pro-1-positive cell counts in the AMs of HCA rats, confirming that HCA induced pyroptosis in these cells. However, MB injection significantly reduced cellular pyroptosis levels (Figure 6A). Additionally, the levels of NLRP3 inflammasome-associated proteins (NLRP3, caspase-1, and ASC) and the pyroptosis-associated protein GSDMD-N were notably elevated in the AMs of HCA rats. In contrast, MB injection markedly suppressed NLRP3 inflammasome activation and pyroptosis (Figures 6B–6F). These findings indicate that HCA triggers NLRP3 inflammasome activation and pyroptosis in rat AMs, while MB effectively inhibits this process.

ML385 and Nigericin partially revert to MB to inhibit HCA-induced pyroptosis of rat lung macrophages and ameliorate lung injury

To further investigate whether MB exerts a protective effect by inhibiting NLRP3 inflammasome activation and activating the Nrf2/HO-1 pathway, we evaluated the effects of the Nrf2 agonist TB, the Nrf2 inhibitor ML, the NLRP3 agonist Nig, and the NLRP3 inhibitor MCC on MB's activity. TB injection significantly increased Nrf2 and HO-1 protein levels in HCA+MB rats, whereas ML injection markedly

reduced them, confirming that intraperitoneal administration of TB or ML effectively modulates the Nrf2/HO-1 pathway in lung tissues (Figures 7A–7C). Similarly, Nig injection increased NLRP3 levels in HCA+MB rats, whereas MCC injection decreased them, indicating that Nig and MCC effectively regulate NLRP3 inflammasome activation (Figure 7D). Notably, TB injection reduced NLRP3 inflammasome-associated protein levels, GSDMD-N expression, and Yo-Pro-1-positive cell counts in AMs from HCA+MB rats. In contrast, ML injection led to increased protein levels and pyroptotic cell counts, suggesting that MB inhibits NLRP3 inflammasome activation and pyroptosis by stimulating the Nrf2/HO-1 pathway. Similarly, Nig injection promoted NLRP3 inflammasome activation and pyroptosis in AMs from HCA+MB rats, whereas MCC had the opposite effect (Figures 7E–7F). Furthermore, TB or MCC administration reduced lung histopathological damage, pathological scores, and ROS levels in HCA+MB rats, while ML or Nig exacerbated these effects (Figures 7G–7H). In the BALF, TNF- α , IL-6, and ICAM-1 levels were significantly reduced, and IL-10 levels were increased after TB or MCC injection, indicating that activating the Nrf2/HO-1 pathway or inhibiting NLRP3 inflammasome activation both alleviated the HCA-induced inflammatory response. Conversely, ML or Nig injection further intensified inflammation (Figures 7I–7L). Overall, these findings demonstrate that MB mitigates HCA-induced histopathological damage, inflammation, and oxidative stress in rat lung tissue by stimulating the Nrf2/HO-1 pathway and inhibiting NLRP3 inflammasome activation.

DISCUSSION

Our results suggest that HCA surgery induces ALI in rats, leading to lung histopathological damage, inflammatory responses, and oxidative stress injury. Additionally, most AMs following HCA were of the M1 type, and the Nrf2/HO-1 pathway was inhibited in lung tissues, triggering AM pyroptosis and NLRP3

inflammasome activation. MB protected rats from HCA-induced lung damage by reducing inflammation and oxidative stress, promoting the conversion of AMs to the M2 type, activating the Nrf2/HO-1 pathway, and inhibiting both AM pyroptosis and NLRP3 inflammasome activation. Importantly, Nrf2 inhibitors and NLRP3 agonists worsened lung injury, whereas Nrf2 agonists and NLRP3 inhibitors enhanced MB's protective effects. Therefore, this study is the first to demonstrate that MB can hinder NLRP3 inflammasome activation by activating the Nrf2/HO-1 pathway, thereby mitigating HCA-induced lung histopathological damage, pyroptosis of AMs, oxidative stress, and inflammation.

HCA-associated lung injury involves complex physiological and pathological processes, including inflammatory responses, oxidative stress, and ischemia-reperfusion injury [44]. MB acts as an antioxidant that reduces oxidative stress and has potential neuroprotective effects [45, 46]. A cohort study showed that push administration of MB (1–2 mg/kg) improves MAP and reduces norepinephrine levels in patients with extracorporeal circulation postvascular paraplegia syndrome after complex cardiac surgery. Patients with higher MAP responded better to MB, suggesting it should be administered before severe hypotension develops [31]. Additionally, a single intravenous injection of MB (1 mg/kg) 30 minutes after traumatic brain injury in rats improved motor function [47]. We established an HCA rat model based on the methods of Linardi et al. [34] and Li et al. [35] and administered MB (1 mg/kg) via push injection 15 minutes before inducing HCA to assess its potential protective effects. MB improved MAP and hematological parameters in HCA rats while alleviating lung tissue damage, suggesting its protective role in lung injury. Moreover, MB has a strong safety profile. A randomized controlled trial found that intravenous infusion of 100 mg MB (dissolved in 500 mL saline) within 24 hours of septic shock diagnosis shortened the duration of vasopressor use and ICU stay, with no serious adverse effects reported [21]. Another study assessing MB's effects and toxicity (0–80 mg/kg) on circulation and metabolism

in rats found that doses up to 20 mg/kg had no adverse effects [48]. Taken together, these findings suggest that MB has strong potential for clinical application.

The vascular endothelium serves as the first barrier to lung tissue, preventing inflammatory cells from migrating into the interstitium and alveolar cells. Disruption of endothelial integrity leads to inflammatory cell infiltration and pulmonary edema[49]. Pulmonary ischemia-reperfusion during CPB has been shown to trigger excessive ROS production, activate the monocyte/macrophage system, and stimulate the release of large quantities of inflammatory cytokines and chemokines (e.g., ICAM-1, TNF- α , and IL-6), further promoting neutrophil recruitment into lung tissue[50]. Notably, Abreu et al. demonstrated that MB mitigates lung inflammation and apoptosis caused by non-ischemic ischemia-reperfusion injury following unilateral lung transplantation in rats[51]. In our study, MB effectively reduced inflammatory infiltration in lung tissues of HCA rats, alleviated alveolar epithelial cell injury and pulmonary edema, and enhanced antioxidant enzyme activity. These findings suggest that MB attenuates lung inflammation and oxidative stress injury caused by HCA, consistent with the study by Abreu et al [51]. A previous study reported that intravenous administration of 9 mg/kg of chlorogenic acid 20 minutes before modeling in deep hypothermic circulatory arrest rats ameliorated brain tissue injury and reduced plasma TNF- α levels from 15 pg/mL to approximately 7 pg/mL [52]. In our study, administration of 1 mg/kg of MB reduced TNF- α levels in BALF from 267 pg/mL to approximately 165 pg/mL. However, due to differences in animal models and assays, direct comparison is not feasible. Importantly, it has been shown that infusion of 3 mg/kg of MB alleviates oleic acid-induced ALI and reduces pulmonary edema in rats [53], further confirming MB's protective effect against lung injury. Macrophage polarization is a process in which macrophages adapt their phenotype to restore homeostasis and enhance their ability to respond to environmental changes[54]. Classically activated M1 macrophages express markers such as CD80, iNOS, and CD86 and exhibit pro-inflammatory properties, while

selectively activated M2 macrophages express markers such as CD163, CD64, and IL-10 and possess anti-inflammatory capabilities[55]. During the acute phase of ALI, AMs predominantly polarize toward the M1 phenotype, releasing large amounts of inflammatory factors that exacerbate the inflammatory response[56]. Our findings support this, as the majority of AMs in the BALF of HCA rats were of the M1 type, with almost no M2 macrophages detected. However, MB treatment significantly increased the proportion of M2-type AMs, suggesting that MB may reduce inflammatory lung injury by promoting AM polarization toward the M2 phenotype.

Cellular pyroptosis is a Caspase-1 or Caspase-11/4/5-dependent form of cell death, primarily characterized by the release of inflammatory mediators, cytoplasmic membrane pore formation, and cell swelling and rupture [57]. This process typically begins with the activation of pathogen recognition receptors (e.g., NLRP3), leading to inflammasome formation. Subsequently, pro-Caspase-1 undergoes autohydrolysis to form mature Caspase-1, which induces membrane pore formation and inflammatory mediator release, ultimately triggering an inflammatory response [58, 59]. It has been reported that blood contact with abiotic surfaces during HCA stimulates the release of inflammatory mediators, activates the NLRP3 inflammasome and Caspase-1, and induces alveolar cell pyroptosis [60]. Additionally, the NLRP3 inflammasome has been implicated in oxygen-glucose deprivation and reoxygenation injury associated with HCA [61]. Thus, inhibiting pyroptosis-related molecules (e.g., NLRP3, Caspase-1) could effectively reduce pyroptosis and inflammation triggered by CPB and HCA. In our study, HCA led to NLRP3 inflammasome activation and cellular pyroptosis in rat AMs, whereas MB treatment inhibited this effect. This inhibition may be a key mechanism underlying MB's lung-protective effects. Several studies have shown that activation of the Nrf2/HO-1 pathway slows the progression of inflammatory diseases and protects lung tissue from injury [30, 62]. For example, Jawad et al. found that activation of this pathway in renal tissue attenuated ischemia-reperfusion injury induced by asphyxial cardiac arrest in rats [63]. Similarly,

Luo et al. demonstrated that the Keap1-Nrf2/HO-1 pathway regulates lipopolysaccharide-induced ALI, and its activation reduces inflammation and ferroptosis in lung tissue [64]. While the pathogenesis of HCA-induced ALI remains unclear, previous studies have implicated the Nrf2 pathway in HCA-induced acute kidney injury [35]. In our research, HCA significantly reduced Nrf2/HO-1 pathway-associated protein levels in rats, supporting its involvement in HCA-induced ALI and aligning with earlier findings [64]. Notably, activation of the Nrf2/HO-1 pathway has also been shown to inhibit NLRP3 inflammasome activation and promote M2-type microglia polarization [65]. Given the importance of the Nrf2/HO-1 pathway, we hypothesized that MB exerts a protective effect against lung damage in HCA rats by activating this pathway. Our findings confirmed this hypothesis, as MB treatment increased Nrf2 and HO-1 levels, demonstrating its ability to activate the Nrf2/HO-1 pathway. Furthermore, Nrf2 inhibitors and NLRP3 agonists exacerbated pyroptosis and inflammasome activation while diminishing MB's protective effects. Conversely, Nrf2 agonists and NLRP3 inhibitors enhanced MB's effects. These results confirm that MB inhibits cellular pyroptosis by activating the Nrf2/HO-1 pathway and suppressing NLRP3 inflammasome activation, thereby reducing inflammation and oxidative stress-induced lung injury in HCA. Previous research has shown that MB protects vascular neurons by activating the PI3K-Akt pathway and ameliorates cognitive deficits caused by chronic cerebral hypoperfusion [66]. Additionally, MB reduces neuroinflammation after subarachnoid hemorrhage via the Akt/GSK-3 β /MEF2D signaling pathway [67]. However, whether these signaling pathways play a role in HCA-induced ALI remains unknown. Future studies should explore whether MB improves HCA-induced ALI through modulation of these pathways.

CONCLUSION

In summary, MB exerts a protective effect against lung damage in HCA rats by promoting the polarization of AMs to the M2 type and reducing cellular pyroptosis. Its mechanism of action appears to be linked to the activation of the Nrf2/HO-1 pathway and the suppression of the NLRP3 inflammasome. This study elucidates the potential mechanism through which MB ameliorates lung injury in HCA rats, expands our understanding of the molecular processes underlying CPB-HCA-induced ALI, and provides a theoretical foundation and data support for the use of MB in treating CPB-HCA-induced ALI. However, there are some limitations to our study that should be noted. First, we did not investigate the dose-dependent effects of MB. Although our chosen doses were based on previously reported data, different doses might yield significantly different outcomes. Future studies will explore the dose-response relationship of MB in greater detail. Additionally, in clinical settings, patients undergoing CPB surgery often have comorbidities such as hypertension, diabetes, and other systemic dysfunctions. To enhance the clinical relevance of our findings, future research should incorporate more complex experimental designs, including HCA models in hypertensive or diabetic animals.

Conflicts of interest: Authors declare no conflicts of interest.

Funding: Authors received no specific funding for this work.

Data availability: To acquire the data that underpins the results of this study, please contact the corresponding author, [TBF].

Submitted: 11 December 2024

Accepted: 29 January 2024

Published online: 13 February 2025

REFERENCES

- [1] Tveita T, Sieck GC. Physiological Impact of Hypothermia: The Good, the Bad, and the Ugly. *Physiology* (Bethesda). 2022;37(2):69-87. <http://doi.org/10.1152/physiol.00025.2021>.
- [2] Ramadoss N, Dharmapuram AK, Goutami V, Verma S. Avoiding use of total circulatory arrest in the practice of congenital heart surgery. *Indian journal of thoracic and cardiovascular surgery*. 2021;37(Suppl 1):174-82. <http://doi.org/10.1007/s12055-020-00955-8>.
- [3] Tan SZ, Singh S, Austin NJ, Alfonso Palanca J, Jubouri M, Girardi LN, et al. Duration of deep hypothermic circulatory arrest for aortic arch surgery: is it a myth, fiction, or scientific leap? *J Cardiovasc Surg (Torino)*. 2022;63(3):243-53. <http://doi.org/10.23736/s0021-9509.22.12275-5>.
- [4] Ghia S, Savadjian A, Shin D, Diluozzo G, Weiner MM, Bhatt HV. Hypothermic Circulatory Arrest in Adult Aortic Arch Surgery: A Review of Hypothermic Circulatory Arrest and its Anesthetic Implications. *J Cardiothorac Vasc Anesth*. 2023;37(12):2634-45. <http://doi.org/10.1053/j.jvca.2023.08.139>.
- [5] Massoth C, Zarbock A, Meersch M. Acute Kidney Injury in Cardiac Surgery. *Crit Care Clin*. 2021;37(2):267-78. <http://doi.org/10.1016/j.ccc.2020.11.009>.
- [6] Gilbey T, Milne B, de Somer F, Kunst G. Neurologic complications after cardiopulmonary bypass - A narrative review. *Perfusion*. 2023;38(8):1545-59. <http://doi.org/10.1177/02676591221119312>.
- [7] Nteliopoulos G, Nikolakopoulou Z, Chow BHN, Corless R, Nguyen B, Dimarakis I. Lung injury following cardiopulmonary bypass: a clinical update. *Expert Rev Cardiovasc Ther*. 2022;20(11):871-80. <http://doi.org/10.1080/14779072.2022.2149492>.
- [8] Cooney SJ, Klawitter J, Khailova L, Robison J, Jaggars J, Ing RJ, et al. Regional lung metabolic profile in a piglet model of cardiopulmonary bypass with circulatory arrest. *Metabolomics*. 2021;17(10):89. <http://doi.org/10.1007/s11306-021-01842-y>.
- [9] Kong M, Wei D, Li X, Zhu X, Hong Z, Ni M, et al. The dynamic changes in autophagy activity and its role in lung injury after deep hypothermic circulatory arrest. *J Cell Mol Med*. 2022;26(4):1113-27. <http://doi.org/10.1111/jcmm.17165>.
- [10] Long ME, Mallampalli RK, Horowitz JC. Pathogenesis of pneumonia and acute lung injury. *Clin Sci (Lond)*. 2022;136(10):747-69. <http://doi.org/10.1042/CS20210879>.
- [11] Xia L, Zhang C, Lv N, Liang Z, Ma T, Cheng H, et al. AdMSC-derived exosomes alleviate acute lung injury via transferring mitochondrial component to improve homeostasis of alveolar macrophages. *Theranostics*. 2022;12(6):2928-47. <http://doi.org/10.7150/thno.69533>.
- [12] Cheng P, Li S, Chen H. Macrophages in Lung Injury, Repair, and Fibrosis. *Cells*. 2021;10(2):436. <http://doi.org/10.3390/cells10020436>.
- [13] Jiao Y, Zhang T, Zhang C, Ji H, Tong X, Xia R, et al. Exosomal miR-30d-5p of neutrophils induces M1 macrophage polarization and primes macrophage

- pyroptosis in sepsis-related acute lung injury. *Crit Care*. 2021;25(1):356. <http://doi.org/10.1186/s13054-021-03775-3>.
- [14] Rao Z, Zhu Y, Yang P, Chen Z, Xia Y, Qiao C, et al. Pyroptosis in inflammatory diseases and cancer. *Theranostics*. 2022;12(9):4310-29. <http://doi.org/10.7150/thno.71086>.
- [15] Ashrafizadeh M. Cell Death Mechanisms in Human Cancers: Molecular Pathways, Therapy Resistance and Therapeutic Perspective. *Journal of Cancer Biomoleculars and Therapeutics*. 2024;1(1):17-40. <http://doi.org/10.62382/jcvt.v1i1.13>.
- [16] Jiang Y, Gao S, Chen Z, Zhao X, Gu J, Wu H, et al. Pyroptosis in septic lung injury: Interactions with other types of cell death. *Biomed Pharmacother*. 2023;169:115914. <http://doi.org/10.1016/j.biopha.2023.115914>.
- [17] Jorquera G, Russell J, Monsalves-Álvarez M, Cruz G, Valladares-Ide D, Basualto-Alarcón C, et al. NLRP3 Inflammasome: Potential Role in Obesity Related Low-Grade Inflammation and Insulin Resistance in Skeletal Muscle. *Int J Mol Sci*. 2021;22(6):3254. <http://doi.org/10.3390/ijms22063254>.
- [18] de Deus IJ, Martins-Silva AF, Fagundes MMA, Paula-Gomes S, Silva F, da Cruz LL, et al. Role of NLRP3 inflammasome and oxidative stress in hepatic insulin resistance and the ameliorative effect of phytochemical intervention. *Front Pharmacol*. 2023;14:1188829. <http://doi.org/10.3389/fphar.2023.1188829>.
- [19] Coll RC, Schroder K, Pelegrin P. NLRP3 and pyroptosis blockers for treating inflammatory diseases. *Trends Pharmacol Sci*. 2022;43(8):653-68. <http://doi.org/10.1016/j.tips.2022.04.003>.
- [20] Xue H, Thaivalappil A, Cao K. The Potentials of Methylene Blue as an Anti-Aging Drug. *Cells*. 2021;10(12):3379. <http://doi.org/10.3390/cells10123379>.
- [21] Ibarra-Estrada M, Kattan E, Aguilera-González P, Sandoval-Plascencia L, Rico-Jauregui U, Gómez-Partida CA, et al. Early adjunctive methylene blue in patients with septic shock: a randomized controlled trial. *Crit Care*. 2023;27(1):110. <http://doi.org/10.1186/s13054-023-04397-7>.
- [22] Pushparajah Mak RS, Liebelt EL. Methylene Blue: An Antidote for Methemoglobinemia and Beyond. *Pediatr Emerg Care*. 2021;37(9):474-7. <http://doi.org/10.1097/pec.0000000000002526>.
- [23] Saha BK, Burns SL. The Story of Nitric Oxide, Sepsis and Methylene Blue: A Comprehensive Pathophysiologic Review. *Am J Med Sci*. 2020;360(4):329-37. <http://doi.org/10.1016/j.amjms.2020.06.007>.
- [24] Gureev AP, Sadovnikova IS, Popov VN. Molecular Mechanisms of the Neuroprotective Effect of Methylene Blue. *Biochemistry (Mosc)*. 2022;87(9):940-56. <http://doi.org/10.1134/S0006297922090073>.
- [25] Ou G, Che J, Dong J, Deng Y, Jiang X, Sun Y, et al. Methylene blue targets PHD3 expression in murine microglia to mitigate lipopolysaccharide-induced neuroinflammation and neurocognitive impairments. *Int Immunopharmacol*. 2023;120:110349. <http://doi.org/10.1016/j.intimp.2023.110349>.

- [26] He F, Ru X, Wen T. NRF2, a Transcription Factor for Stress Response and Beyond. *Int J Mol Sci.* 2020;21(13):4777. <http://doi.org/10.3390/ijms21134777>.
- [27] Liu Y, Wang S, Jin G, Gao K, Wang S, Zhang X, et al. Network pharmacology-based study on the mechanism of ShenKang injection in diabetic kidney disease through Keap1/Nrf2/Ho-1 signaling pathway. *Phytomedicine.* 2023;118:154915. <http://doi.org/10.1016/j.phymed.2023.154915>.
- [28] Sun YY, Zhu HJ, Zhao RY, Zhou SY, Wang MQ, Yang Y, et al. Remote ischemic conditioning attenuates oxidative stress and inflammation via the Nrf2/HO-1 pathway in MCAO mice. *Redox biology.* 2023;66:102852. <http://doi.org/10.1016/j.redox.2023.102852>.
- [29] Sha W, Zhao B, Wei H, Yang Y, Yin H, Gao J, et al. Astragalus polysaccharide ameliorates vascular endothelial dysfunction by stimulating macrophage M2 polarization via potentiating Nrf2/HO-1 signaling pathway. *Phytomedicine.* 2023;112:154667. <http://doi.org/10.1016/j.phymed.2023.154667>.
- [30] Zhang Q, Liu J, Duan H, Li R, Peng W, Wu C. Activation of Nrf2/HO-1 signaling: An important molecular mechanism of herbal medicine in the treatment of atherosclerosis via the protection of vascular endothelial cells from oxidative stress. *Journal of advanced research.* 2021;34:43-63. <http://doi.org/10.1016/j.jare.2021.06.023>.
- [31] Mazzeffi M, Hammer B, Chen E, Caridi-Scheible M, Ramsay J, Paciullo C. Methylene blue for postcardiopulmonary bypass vasoplegic syndrome: A cohort study. *Ann Card Anaesth.* 2017;20(2):178-81. http://doi.org/10.4103/aca.ACA_237_16.
- [32] Zhang J, Li J, An Z, Qi J. Hydromorphone Mitigates Cardiopulmonary Bypass-Induced Acute Lung Injury by Repressing Pyroptosis of Alveolar Macrophages. *Shock.* 2023;60(1):92-9. <http://doi.org/10.1097/SHK.0000000000002138>.
- [33] Zhang L, Jiang YH, Fan C, Zhang Q, Jiang YH, Li Y, et al. MCC950 attenuates doxorubicin-induced myocardial injury in vivo and in vitro by inhibiting NLRP3-mediated pyroptosis. *Biomed Pharmacother.* 2021;143:112133. <http://doi.org/10.1016/j.biopha.2021.112133>.
- [34] Linardi D, Walpoth B, Mani R, Murari A, Tessari M, Hoxha S, et al. Slow versus fast rewarming after hypothermic circulatory arrest: effects on neuroinflammation and cerebral oedema. *Eur J Cardiothorac Surg.* 2020;58(4):792-800. <http://doi.org/10.1093/ejcts/ezaa143>.
- [35] Li J, Wang M, Wang M, Sang H, Wang W, Gong M, et al. Bradykinin induces acute kidney injury after hypothermic circulatory arrest through the repression of the Nrf2-xCT pathway. *iScience.* 2024;27(6):110075. <http://doi.org/10.1016/j.isci.2024.110075>.
- [36] Kalidhindi RSR, Ambhore NS, Sathish V. Cellular and Biochemical Analysis of Bronchoalveolar Lavage Fluid from Murine Lungs. *Methods Mol Biol.* 2021;2223:201-15. http://doi.org/10.1007/978-1-0716-1001-5_15.
- [37] Hirao S, Minakata K, Masumoto H, Yamazaki K, Ikeda T, Minatoya K, et al. Recombinant human soluble thrombomodulin prevents acute lung injury in a rat

- cardiopulmonary bypass model. *J Thorac Cardiovasc Surg.* 2017;154(6):1973-83 e1. <http://doi.org/10.1016/j.jtcvs.2017.05.051>.
- [38] Lin L, Zhang L, Yu L, Han L, Ji W, Shen H, et al. Time-dependent changes of autophagy and apoptosis in lipopolysaccharide-induced rat acute lung injury. *Iran J Basic Med Sci.* 2016;19(6):632-7.
- [39] Hwang S, Sung DK, Kim YE, Yang M, Ahn SY, Sung SI, et al. Mesenchymal Stromal Cells Primed by Toll-like Receptors 3 and 4 Enhanced Anti-Inflammatory Effects against LPS-Induced Macrophages via Extracellular Vesicles. *Int J Mol Sci.* 2023;24(22):16264. <http://doi.org/10.3390/ijms242216264>.
- [40] Dai S, Ji J, Li R, Gao L, He X. Stellate Ganglion Block Attenuates LPS-Induced Acute Lung Injury by Activating Sirt3 Regulation of Oxidative Stress and Inflammation. *Biomedicines.* 2024;12(6):1148. <http://doi.org/10.3390/biomedicines12061148>.
- [41] Han X, Xu T, Fang Q, Zhang H, Yue L, Hu G, et al. Quercetin hinders microglial activation to alleviate neurotoxicity via the interplay between NLRP3 inflammasome and mitophagy. *Redox Biol.* 2021;44:102010. <http://doi.org/10.1016/j.redox.2021.102010>.
- [42] Zhong WJ, Liu T, Yang HH, Duan JX, Yang JT, Guan XX, et al. TREM-1 governs NLRP3 inflammasome activation of macrophages by firing up glycolysis in acute lung injury. *Int J Biol Sci.* 2023;19(1):242-57. <http://doi.org/10.7150/ijbs.77304>.
- [43] Liu B, He R, Zhang L, Hao B, Jiang W, Wang W, et al. Inflammatory Caspases Drive Pyroptosis in Acute Lung Injury. *Front Pharmacol.* 2021;12:631256. <http://doi.org/10.3389/fphar.2021.631256>.
- [44] Zheng XM, Yang Z, Yang GL, Huang Y, Peng JR, Wu MJ. Lung injury after cardiopulmonary bypass: Alternative treatment prospects. *World journal of clinical cases.* 2022;10(3):753-61. <http://doi.org/10.12998/wjcc.v10.i3.753>.
- [45] Tucker D, Lu Y, Zhang Q. From Mitochondrial Function to Neuroprotection-an Emerging Role for Methylene Blue. *Mol Neurobiol.* 2018;55(6):5137-53. <http://doi.org/10.1007/s12035-017-0712-2>.
- [46] Mai H, Liu C, Fu B, Ji X, Chen M, Zhang Y, et al. Methylene Blue Reduces Retinal Cell Inflammation, Apoptosis, and Oxidative Stress in a Rat Model of Diabetic Retinopathy via Sirtuin 1 Activation. *Altern Ther Health Med.* 2023;29(8):156-65.
- [47] Genrikhs EE, Stelmashook EV, Voronkov DN, Novikova SV, Alexandrova OP, Gulyaev MV, et al. The Delayed Neuroprotective Effect of Methylene Blue in Experimental Rat Brain Trauma. *Antioxidants (Basel, Switzerland).* 2020;9(5):377. <http://doi.org/10.3390/antiox9050377>.
- [48] Haouzi P, Gueguinou M, Sonobe T, Judenherc-Haouzi A, Tubbs N, Trebak M, et al. Revisiting the physiological effects of methylene blue as a treatment of cyanide intoxication. *Clin Toxicol (Phila).* 2018;56(9):828-40. <http://doi.org/10.1080/15563650.2018.1429615>.

- [49] Vlastos D, Zeinah M, Ninkovic-Hall G, Vlachos S, Salem A, Asonitis A, et al. The effects of ischaemic conditioning on lung ischaemia-reperfusion injury. *Respir Res.* 2022;23(1):351. <http://doi.org/10.1186/s12931-022-02288-z>.
- [50] Sun H, Zhao X, Tai Q, Xu G, Ju Y, Gao W. Endothelial colony-forming cells reduced the lung injury induced by cardiopulmonary bypass in rats. *Stem Cell Res Ther.* 2020;11(1):246. <http://doi.org/10.1186/s13287-020-01722-7>.
- [51] Abreu MDM, Almeida FM, Santos KBD, Assis E, Hamada RKF, Jatene FB, et al. Does methylene blue attenuate inflammation in nonischemic lungs after lung transplantation? *J Bras Pneumol.* 2018;44(5):378-82. <http://doi.org/10.1590/S1806-37562017000000172>.
- [52] Chen Q, Lei YQ, Liu JF, Wang ZC, Cao H. Beneficial effects of chlorogenic acid treatment on neuroinflammation after deep hypothermic circulatory arrest may be mediated through CYLD/NF- κ B signaling. *Brain Res.* 2021;1767:147572. <http://doi.org/10.1016/j.brainres.2021.147572>.
- [53] Cassiano Silveira AP, Vento DA, Albuquerque AA, Celotto AC, Tefé-Silva C, Ramos SG, et al. Effects of methylene blue in acute lung injury induced by oleic acid in rats. *Annals of translational medicine.* 2016;4(1):8. <http://doi.org/10.3978/j.issn.2305-5839.2015.12.51>.
- [54] Deng L, Jian Z, Xu T, Li F, Deng H, Zhou Y, et al. Macrophage Polarization: An Important Candidate Regulator for Lung Diseases. *Molecules.* 2023;28(5):2379. <http://doi.org/10.3390/molecules28052379>.
- [55] Wang L, Wang D, Zhang T, Ma Y, Tong X, Fan H. The role of immunometabolism in macrophage polarization and its impact on acute lung injury/acute respiratory distress syndrome. *Front Immunol.* 2023;14:1117548. <http://doi.org/10.3389/fimmu.2023.1117548>.
- [56] Chen X, Tang J, Shuai W, Meng J, Feng J, Han Z. Macrophage polarization and its role in the pathogenesis of acute lung injury/acute respiratory distress syndrome. *Inflamm Res.* 2020;69(9):883-95. <http://doi.org/10.1007/s00011-020-01378-2>.
- [57] Yu P, Zhang X, Liu N, Tang L, Peng C, Chen X. Pyroptosis: mechanisms and diseases. *Signal transduction and targeted therapy.* 2021;6(1):128. <http://doi.org/10.1038/s41392-021-00507-5>.
- [58] Liu B, Wang Z, He R, Xiong R, Li G, Zhang L, et al. Buformin alleviates sepsis-induced acute lung injury via inhibiting NLRP3-mediated pyroptosis through an AMPK-dependent pathway. *Clin Sci (Lond).* 2022;136(4):273-89. <http://doi.org/10.1042/cs20211156>.
- [59] Feng Y, Li M, Yangzhong X, Zhang X, Zu A, Hou Y, et al. Pyroptosis in inflammation-related respiratory disease. *J Physiol Biochem.* 2022;78(4):721-37. <http://doi.org/10.1007/s13105-022-00909-1>.
- [60] Li H, Zhang W, Lou Q, Chang Y, Lin Z, Lou L. XueFu ZhuYu Decoction Alleviates Cardiopulmonary Bypass-Induced NLRP3 Inflammasome-Dependent Pyroptosis by Inhibiting I κ B- α /NF- κ B Pathway in Acute Lung Injury Rats. *Evid Based Complement Alternat Med.* 2022;2022:6248870. <http://doi.org/10.1155/2022/6248870>.

- [61] Kong LY, Zhu SY, Si MY, Xu XH, Yu JJ, Zhong WX, et al. TAK-242 protects against oxygen-glucose deprivation and reoxygenation-induced injury in brain microvascular endothelial cells and alters the expression pattern of lncRNAs. *J Thorac Dis.* 2023;15(5):2571-84. <http://doi.org/10.21037/jtd-23-360>.
- [62] Li J, Lu K, Sun F, Tan S, Zhang X, Sheng W, et al. Panaxydol attenuates ferroptosis against LPS-induced acute lung injury in mice by Keap1-Nrf2/HO-1 pathway. *J Transl Med.* 2021;19(1):96. <http://doi.org/10.1186/s12967-021-02745-1>.
- [63] Jawad A, Yoo YJ, Cho JH, Yoon JC, Tian W, Islam MS, et al. Therapeutic hypothermia effect on asphyxial cardiac arrest-induced renal ischemia/reperfusion injury via change of Nrf2/HO-1 levels. *Exp Ther Med.* 2021;22(3):1031. <http://doi.org/10.3892/etm.2021.10463>.
- [64] Luo L, Huang F, Zhong S, Ding R, Su J, Li X. Astaxanthin attenuates ferroptosis via Keap1-Nrf2/HO-1 signaling pathways in LPS-induced acute lung injury. *Life Sci.* 2022;311(Pt A):121091. <http://doi.org/10.1016/j.lfs.2022.121091>.
- [65] Tao W, Hu Y, Chen Z, Dai Y, Hu Y, Qi M. Magnolol attenuates depressive-like behaviors by polarizing microglia towards the M2 phenotype through the regulation of Nrf2/HO-1/NLRP3 signaling pathway. *Phytomedicine.* 2021;91:153692. <http://doi.org/10.1016/j.phymed.2021.153692>.
- [66] Li Y, Wang X, Liu M, Zhang W, Li R, Nie Z. Effect of Methylene Blue and PI3K-Akt Pathway Inhibitors on the Neurovascular System after Chronic Cerebral Hypoperfusion in Rats. *J Mol Neurosci.* 2020;70(11):1797-807. <http://doi.org/10.1007/s12031-020-01572-1>.
- [67] Xu H, Li J, Wang Z, Feng M, Shen Y, Cao S, et al. Methylene blue attenuates neuroinflammation after subarachnoid hemorrhage in rats through the Akt/GSK-3 β /MEF2D signaling pathway. *Brain Behav Immun.* 2017;65:125-39. <http://doi.org/10.1016/j.bbi.2017.04.020>.

FIGURES WITH LEGENDS

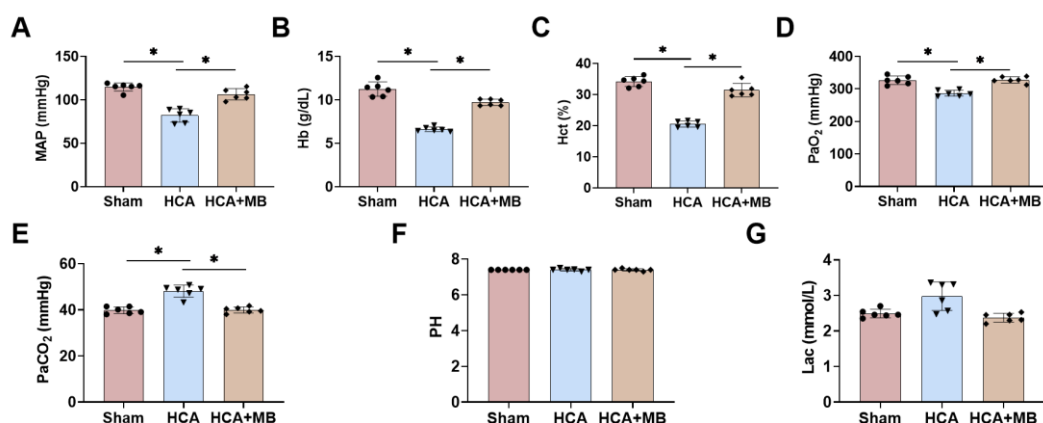


Figure 1. MB ameliorates HCA-induced abnormalities in physiological indices in rats

(A) Mean arterial pressure (MAP) was monitored in rats using a multifunctional physiological monitor 30 min after surgery. Recording of hemoglobin (Hb) (B), hematocrit (Hct) (C), partial pressure of arterial oxygen (PaO₂), (D) partial pressure of arterial blood carbon dioxide (PaCO₂) (E), Pondus Hydrogenii (pH) (F), and lactic acid (Lac) (G) by blood gas analyser. n=6, *P<0.05.

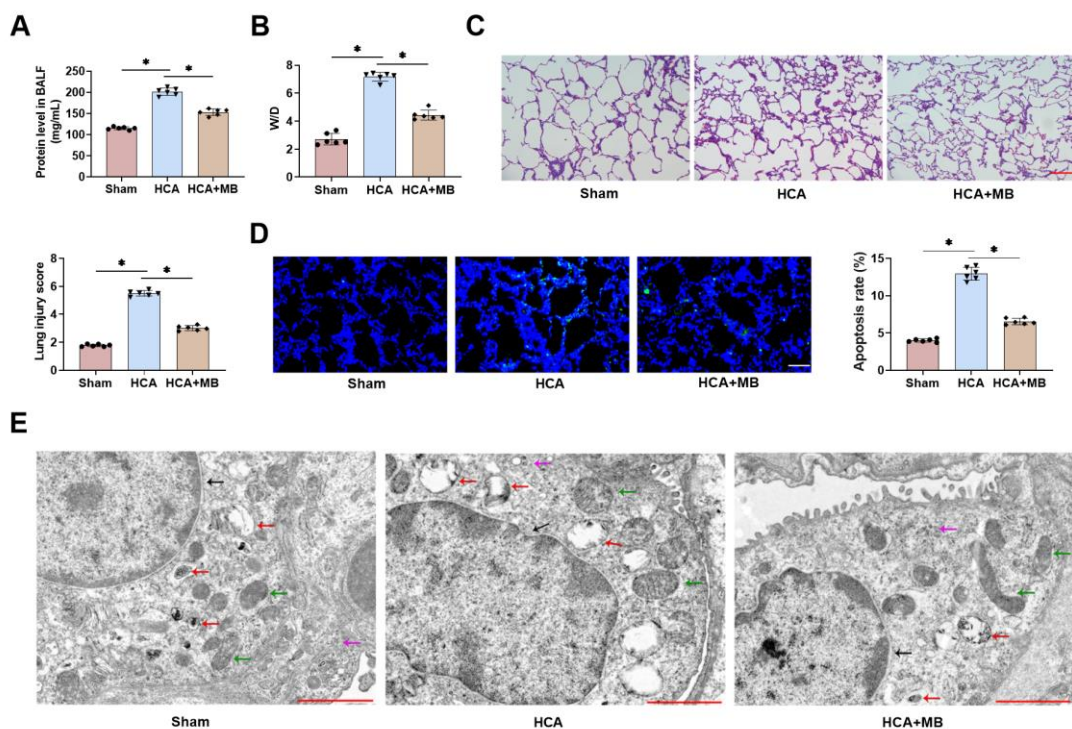


Figure 2. MB ameliorates HCA-induced histopathological lung injury in rats

(A) BALF was gathered and total protein concentration in the supernatant was assessed. (B) Calculated the W/D of lung tissue in rats. (C) The pathological changes in rat lung tissue were assessed by HE staining, and scored lung injury (20×, bar=100 μm). (D) TUNEL fluorescence staining to detect apoptosis rate in lung tissues of rats (40×, bar=50 μm). (E) Transmission electron microscopy revealed ultrastructural changes in lung tissue (6k×, bar=2 μm). n=6, *P<0.05.

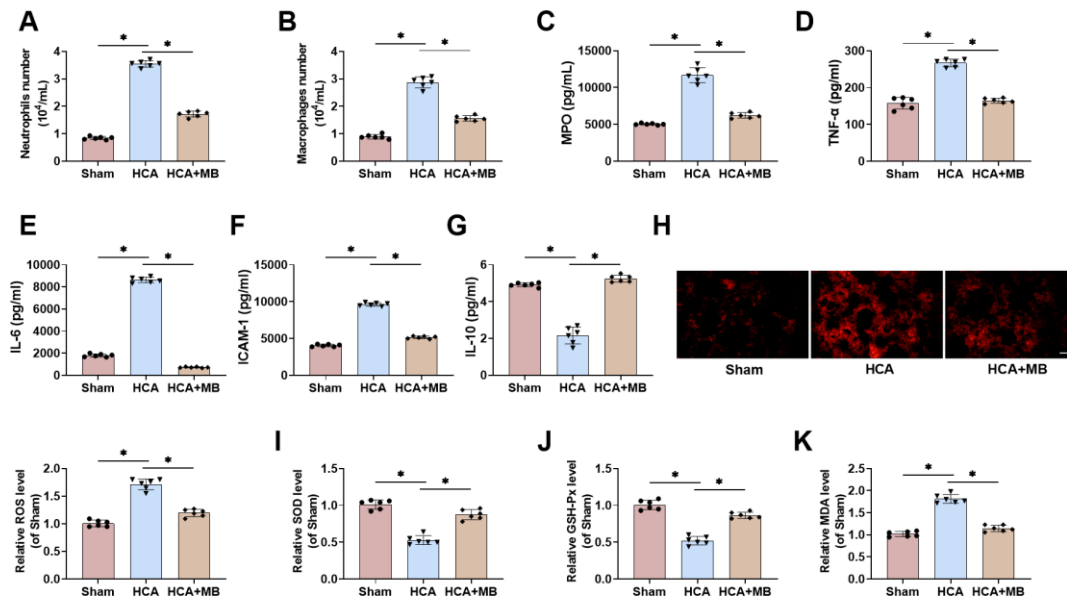


Figure 3. MB ameliorates HCA-induced inflammatory and oxidative stress injury in rat lungs

(A-B) BALF was collected and neutrophil and macrophage counts were calculated. (C) Inflammatory factor MPO level in lung tissue was detected through ELISA kit to assess neutrophil infiltration. (D-G) TNF- α , IL-6, ICAM-1 and anti-inflammatory factor IL-10 levels in BALF were assessed by ELISA kits. (H) The ROS level was measured utilizing DHE staining (20 \times , bar=100 μ m). (I-K) To evaluate oxidative stress, SOD, GSH-Px and MDA levels were assessed by ELISA kits. n=6, * P <0.05.

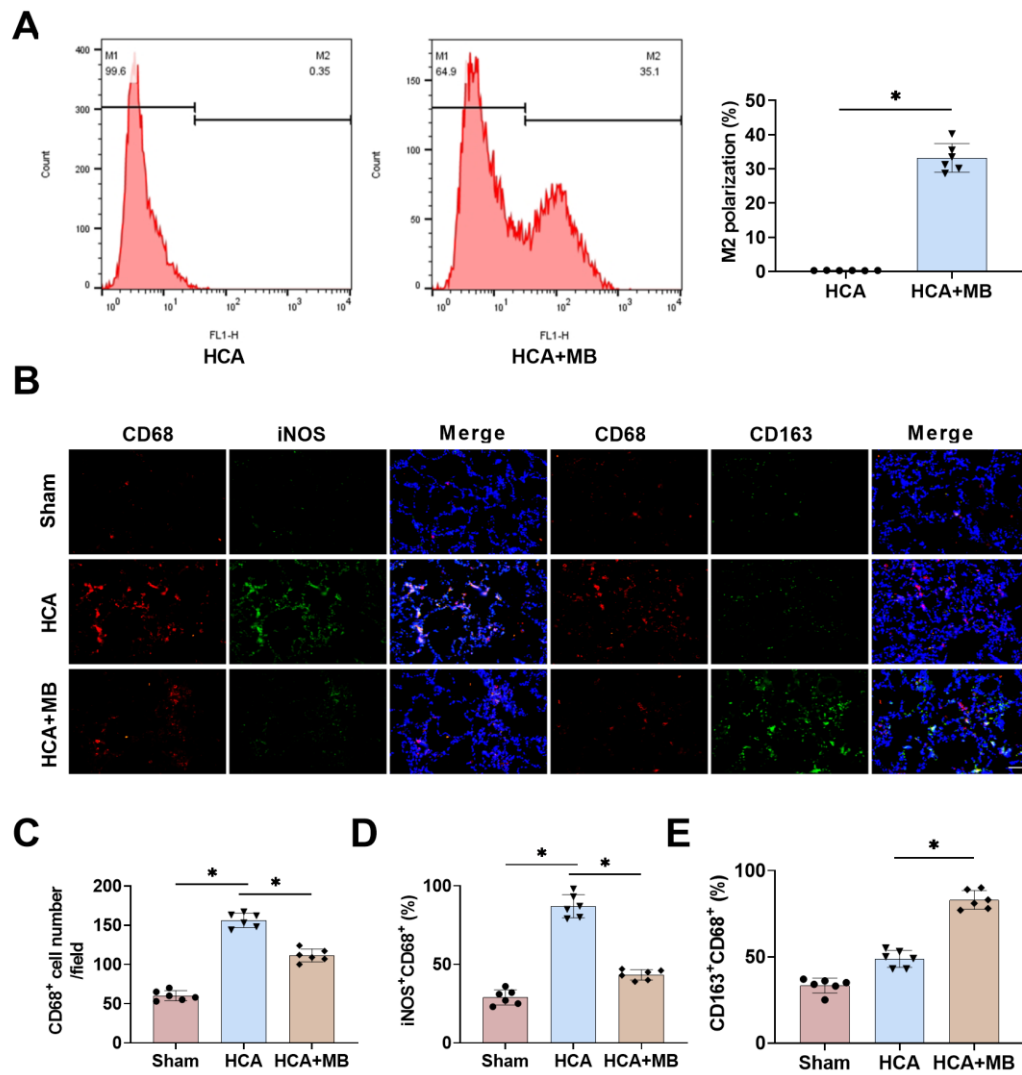


Figure 4. MB can promote HCA-induced polarization of rat AMs to M2

(A) The percentage of AMs polarization were evaluated by Flow cytometry. (B-E) Immunofluorescence double staining to determine the changes in the percentage of M1 and M2 in rat lung tissue (40 \times , bar=50 μ m). n=6, * P <0.05.

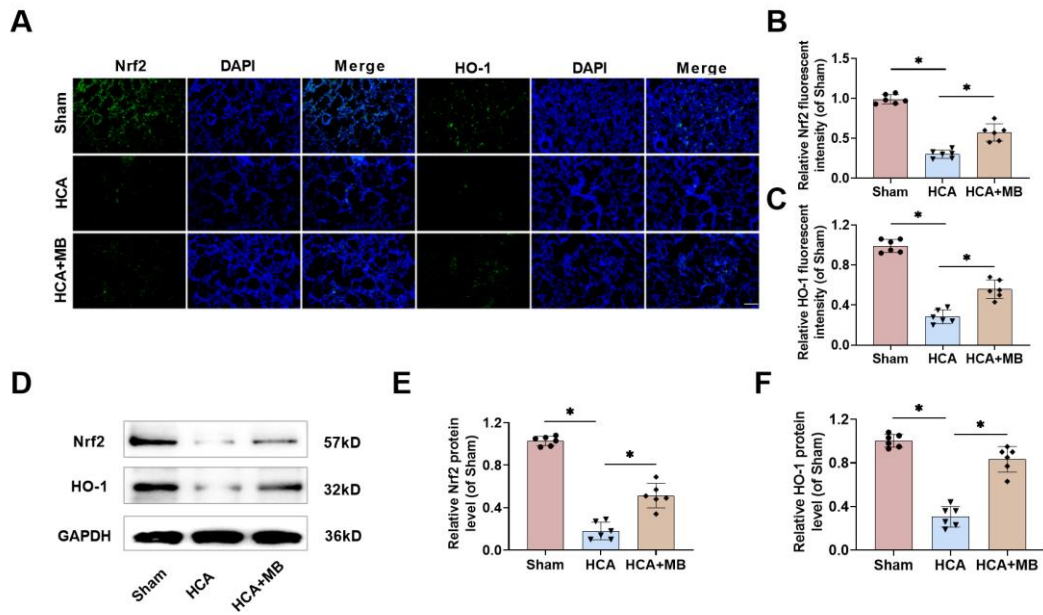


Figure 5. MB can activate Nrf2/HO-1 pathway in HCA rats

(A-C) Nrf2 and HO-1 protein levels in lung tissue were assessed by immunofluorescence staining (20 \times , bar=100 μ m). (D-F) Examining Nrf2 and HO-1 levels in lung tissues through Western blot. n=6, * P <0.05.

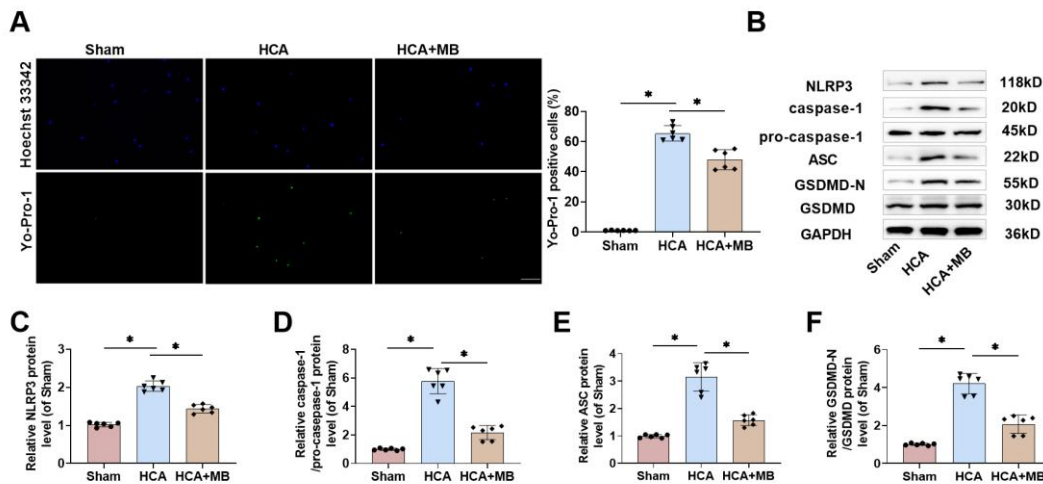


Figure 6. MB inhibits pyroptosis in AMs caused by NLRP3 inflammasome in HCA rats

(A) The pyroptosis level of rat AMs was detected by Yo-Pro-1 staining (green) and Hoechst 33342 staining (nuclear blue) (20 \times , bar=100 μ m). (B-F) Western blot bands

and relative expression levels of NLRP3, caspase-1, pro-caspase-1, ASC, GSDMD-N, and GSDMD in AMs. n=6, * P <0.05.

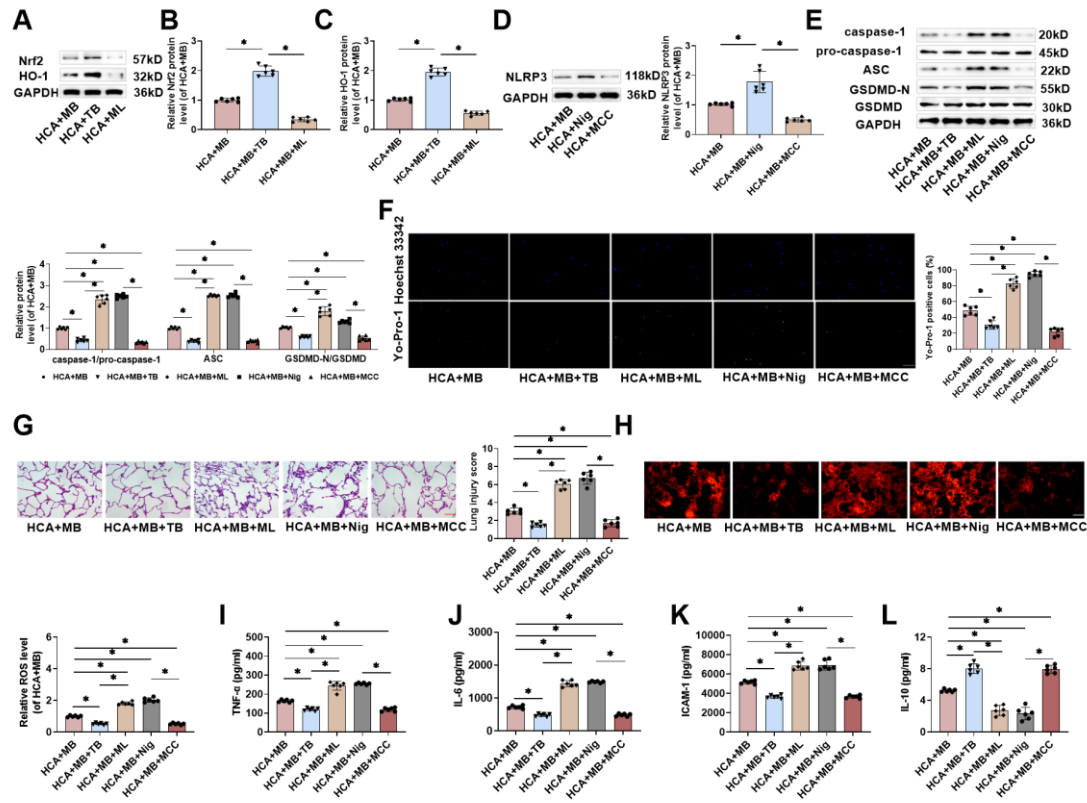


Figure 7. ML385 and Nigericin can partially restore MB to inhibit HCA-induced pyroptosis of rat lung macrophages and improve lung injury

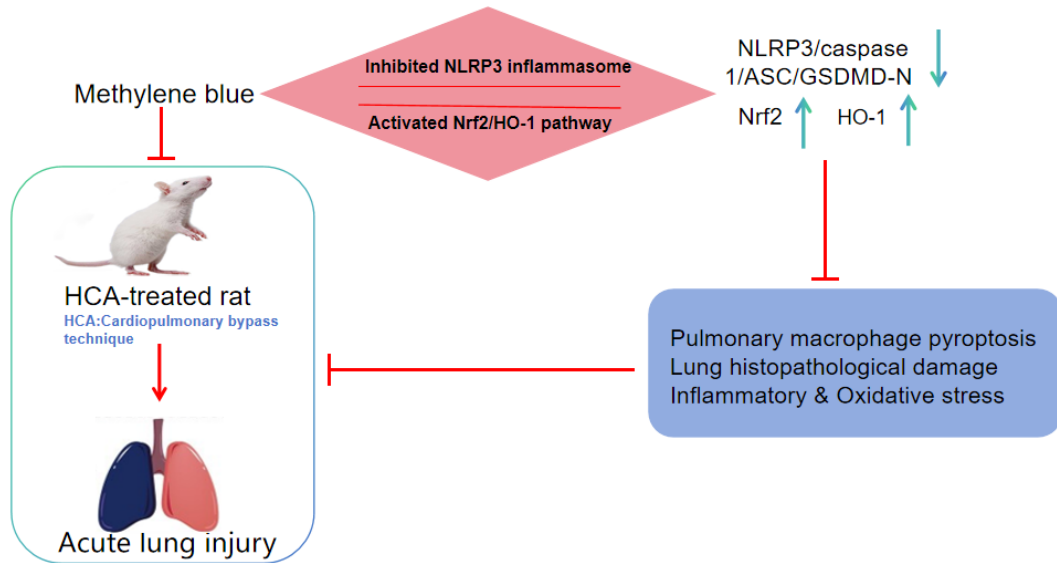
(A-E) Western blot bands and relative levels of NLRP3, caspase-1, pro-caspase-1, ASC, GSDMD-N, and GSDMD in AMs. (F) The pyroptosis level of rat AMs was detected by Yo-Pro-1 staining (green) and Hoechst 33342 staining (nuclear blue) (20 \times , bar=100 μ m). (G) Utilizing HE staining to evaluate the pathological changes in rat lung tissue, and to score lung injury (20 \times , bar=100 μ m). (H) The ROS level was measured utilizing DHE staining (20 \times , bar=100 μ m). (I-L) TNF- α , IL-6, ICAM-1, and IL-10 levels in BALF were assessed using ELISA kits. n=6, * P <0.05.

Highlights:

1. Methylene blue (MB) ameliorates hypothermic circulatory arrest (HCA)-induced lung-related injury in rats.

2. MB promotes HCA-induced polarization of rat alveolar macrophages (AMs) to the M2 type.
3. MB activates the Nrf2/HO-1 pathway in HCA rats.
4. MB inhibits HCA-induced NLRP3 inflammasome-mediated pyroptosis in rat lung tissue AMs.

Graphical abstract



MB activated the Nrf2/HO-1 pathway and inhibited NLRP3 inflammasome activation, promoted the polarization of AMs toward the M2 type, and alleviated cell pyroptosis, ameliorated the pathological damage of lung tissues, inhibited inflammatory responses and oxidative stress, and thus exerted a protective effect against lung injury in HCA rats.